# A micromachined angular-acceleration sensor for geophysical applications

Huafeng Liu and W. T. Pike

Citation: Appl. Phys. Lett. **109**, 173506 (2016); doi: 10.1063/1.4966547
View online: http://dx.doi.org/10.1063/1.4966547
View Table of Contents: http://aip.scitation.org/toc/apl/109/17
Published by the American Institute of Physics

# A micromachined angular-acceleration sensor for geophysical applications

Huafeng Liu[a] and W. T. Pike[b]
*Optical and Semiconductor Devices Group, Department of Electrical and Electronic Engineering, Imperial College London, London SW7 2AZ, United Kingdom*

(Received 14 August 2016; accepted 16 October 2016; published online 26 October 2016)

This paper presents an angular-acceleration sensor that works as either an angular accelerometer or a gravity gradiometer and is based on the micro electromechanical system (MEMS) technology. The changes in the angle of the sensor mass are sensed by a rotational capacitive array transducer that is formed by electrodes on both the stator and rotor dies of the flip-chip-bonded MEMS chip (21 mm × 12.5 mm × 1 mm). The prototype was characterized, demonstrating a fundamental frequency of 27 Hz, a quality factor of 230 in air, and a sensitivity of 6 mV/(rad/s$^2$). The demonstrated noise floor was less than 0.003 rad/s$^2$/$\sqrt{\text{Hz}}$ within a bandwidth of 0.1 Hz to 10 Hz, which is comparable with the conventional angular accelerometer and is better than the other reported MEMS sensors in low-frequency ranges. The features of small size and low cost suggest that this MEMS angular-acceleration sensor could be mounted on a drone, a satellite or even a Mars rover, and it is promising to be used for monitoring angular accelerations, aiding seismic recording, mapping gravity anomalies, and other geophysical applications for large-scale terrestrial and space deployments. *Published by AIP Publishing*. [http://dx.doi.org/10.1063/1.4966547]

Angular-acceleration sensors have broad applications in geophysical fields. During oil and gas explorations, drilling tools generally experience low-frequency torsional-oscillation (LFTO) of less than 5 Hz, which significantly reduces the drilling efficiency and rate of penetration. Therefore, angular-acceleration sensors are integrated to improve the rotary steerable drilling system.[1] In seismic records, the unwanted tilts caused by atmospheric or local effects cannot be separated by a single seismometer because of the equivalence of inertial and gravitational accelerations. Angular-acceleration sensors are used to determine the tilt angles for reducing the effects of sensitivity shifts of a broadband seismometer,[2] typically in a bandwidth of 0.01 Hz to 10 Hz. In addition, a superconducting angular accelerometer was demonstrated for implementing gravity gradiometry.[3] A gravity gradiometer uses the gravity method[4] for oil and mineral exploration, crustal anomaly measurement, and archaeology[5] by determining the gravity gradient of the areas of interest. A typical work bandwidth of a moving-base gravity gradiometer is 0.001 Hz to 1 Hz.[3] Hence, angular-acceleration sensors for those geophysical applications operate at frequencies lower than 10 Hz. Conventionally machined sensors can achieve lower fundamental frequencies for a better sensitivity or response to low-frequency signals. However, for large-scale deployments, cost-efficiency and power-efficiency have to be considered. Hence, angular-acceleration sensors for those geophysical applications require miniaturization and batch fabrication.

Micro electromechanical system (MEMS) technology offers the potential to miniaturize the instruments. MEMS-based sensors have been widely used for automotive, consumer electronics, and aerospace applications.[6] However, MEMS sensors for geophysical applications are emerging in the past two decades. MEMS seismic-grade accelerometers[7–9] have been developed to determine the surface seismic waves for either monitoring earthquakes or subsurface imaging oil exploration using the seismic reflection method,[10] including the 0.2 ng/$\sqrt{\text{Hz}}$ short-period seismometer[11,12] recently developed in our group as a contribution to NASA's InSight Mars mission. There are also several reported MEMS angular accelerometers.[13–15] However, all of them have fundamental frequencies of several hundreds to thousands hertz, therefore none of them have a low noise floor at lower frequencies. This paper presents a MEMS angular-acceleration sensor that works as either an angular accelerometer or a gravity gradiometer, with a much lower fundamental frequency for geophysical applications.

Fig. 1 schematically shows the principle of the angular-acceleration sensor. Two proof masses are symmetrically connected at the ends of a massless solid bar that is suspended by a rotary suspension. The suspension flexure that allows in-plane rotations and rejects other translations and rotations is anchored on the solid frame. When an angular acceleration with an arbitrary rotation center is applied on the sensor frame, a torque is generated about the pivot. This torque is determined by the vector components of the inertial forces along the directions that are perpendicular to the bar

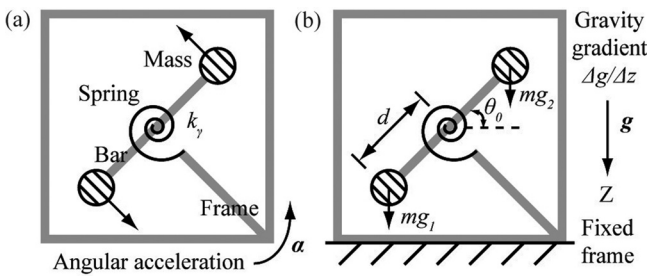


FIG. 1. Principles of the angular-acceleration sensor working as (a) an angular accelerometer or (b) a gravity gradiometer; grey color represents solid structures.

[a]h.liu11@imperial.ac.uk
[b]w.t.pike@imperial.ac.uk

and is independent of the rotation center.[16] The torque can be balanced by the deformation of the suspension flexure with respect to a certain rotation angle which is sensed by a rotational capacitive array transducer (RCAT). In addition, due to the presence of the gravity gradient $\Delta g/\Delta z$ under a gravitational field, a gravity gradient torque (GGT) is produced on the pivot by the difference of gravitational forces applied on the masses that are at different spatial locations. When the sensor frame is fixed on an inertial frame, this GGT induced torsion-balance angle can be observed. The sensor's suspension design and dynamics are described in the prior work.[17] Using the same rotation transducer, the vertical component of the gravity gradient tensor, $\Gamma_{zz}$, can be determined. Hence, this angular-acceleration sensor can be operated as either an angular accelerometer or a gravity gradiometer.

Fig. 2 shows the cross-sectional view of the angular-acceleration sensor with a chip size of 21 mm × 12.5 mm × 1 mm. The sensor chip consists of the stator die on the bottom and the rotor die on the top. The RCAT, which is a rotational variation of the lateral capacitive array transducer (LCAT) previously developed in our group, has periodic electrodes with each electrode in a sector shape. The differential-drive electrodes are located on the stator die, while the pickup electrodes are on the rotor die. When there are relative movements close to the null position of the RCAT, changes in capacitance are proportionally to the rotation angle and are then picked up by the proven front-end circuit of the prior work.[11] The bootstrapping technology[18] has been applied to eliminate the effect of stray capacitors by using guard electrodes, whose voltage potentials are driven to be the same as the pickup electrodes, underneath and opposite to the pickup electrodes. Both the stator and rotor dies were implemented simultaneously by microfabrications on the same 4-in. silicon wafer through four photomasks. First, a silicon wafer with an oxidation layer on top was sputter-coated with 40 nm/400 nm Ti/Au layers that were then patterned by photolithography and etched to form the Metal 1 features. Then, a 1.2 $\mu$m silicon dioxide layer was coated by plasma enhanced chemical vapour deposition (PECVD). Windows for interconnections between the Metal 1 and the Metal 2 layers were opened by reactive ion etching (RIE) of silicon dioxide. Next, 40 nm/5 $\mu$m Ti/Au layers were sputter-coated, electroplated, patterned, and etched to form the Metal 2 and interconnections. Then, a through-wafer deep reactive ion etching (DRIE) process was carried out to form the mechanical structures and dicing-free features. In the end, both the stator and rotor dies were singulated, paired, and then bonded using flip-chip technology with an alignment error of no larger than 0.06°. Then, the MEMS chip was centrally glued on top of the front-end printed circuit board (PCB) and the electrical connections were formed by wire-bonding of gold wires to the fingers of the chip and the PCB (30 mm × 30 mm). A 3D-printed case was installed on the PCB for chip protection, as shown in Fig. 3. Then, the PCB was connected to a conditioning circuit, and the prototype was put into a metal box for suppressing electromagnetic interferences.

When the MEMS chip works as an angular accelerometer, it is sensitive to in-plane angular accelerations $\alpha$, as shown in Figs. 1 and 3. It can be seen as a second-order mass-spring-damping system[19] whose transfer function can be presented as

$$H_{aa}(s) = \frac{\theta(s)}{\alpha(s)} = \frac{1}{s^2 + \frac{b}{I}s + \frac{k_\gamma}{I}} = \frac{1}{s^2 + \frac{\omega_0}{Q}s + \omega_0^2}, \quad (1)$$

where $\theta$ and $\alpha$ are the angular displacement and the angular acceleration applied on the proof mass, $k_\gamma$ and $I$ are the spring constant and the moment of inertia about the rotation axis, and $\omega_0 = 2\pi f_0$, $b$ and $Q$ are the angular fundamental frequency, the damping factor and the quality factor of the device, respectively. For signals with lower frequencies ($\omega \ll \omega_0$), $H_{aa}(s) = I/k_\gamma$. When the sensor chip is fixed on an inertial frame and the square masses are spatially separated along the gravity vector, as shown in Fig. 3, the chip works as a gravity gradiometer. In this case, the in-plane GGT applied on the sensor is balanced by the deformation of the suspension $m(g_1 - g_2)d\sin\theta_0 = k_\gamma\Delta\theta$, where $\Delta\theta$ is the in-plane angular displacement, $\theta_0$ is the initial angle between the mass-connection bar and the gravity vector, and $d$ is a half of the bar length, as illustrated in Fig. 1. The gravity gradient can be determined by $\Delta g/\Delta z = k_\gamma\Delta\theta/(md^2\sin 2\theta_0)$, where z-axis is parallel to the gravity vector, as shown in Fig. 1. The sensitivity of the gradiometer is maximized when $\theta_0$ is equal to 45°, and is less affected by angular misalignments since sine-function has slower slopes at inflection points. In this case, this gradiometer chip has a larger installation misalignment tolerance. For lower frequencies ($\omega \ll \omega_0$), the transfer function of the gravity gradiometer is $H_{gg}(s) = md^2/k_\gamma$. The angular displacements of both cases can be sensed by the RCAT and conditioned by corresponding circuits with an output in voltages. However, in a non-inertial frame, the angular displacement of the gravity gradiometer

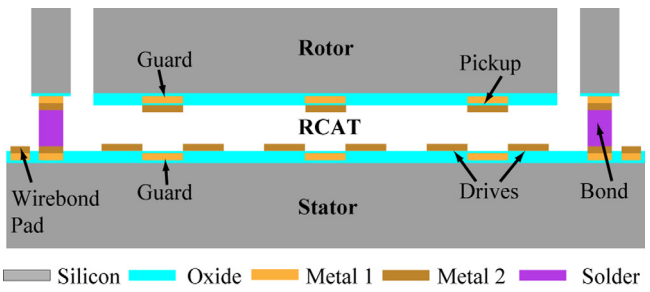


FIG. 2. Cross-sectional sensor diagram when the RCAT is in its null position.

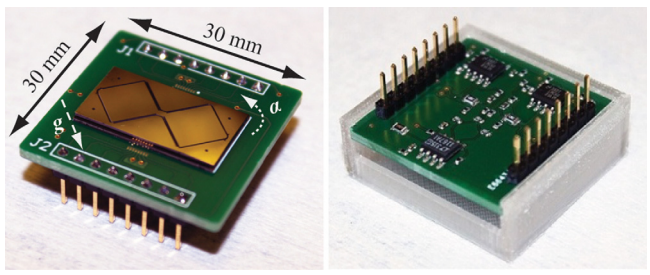


FIG. 3. Front-end PCB (30 mm × 30 mm) with the MEMS chip on the top and the front-end electronics at the bottom.

will be interfered by angular accelerations. In order to solve this issue, two identical gravity-gradiometer chips have to be fixed in a solid frame with the sensing mass of each chip orthogonally paired and the sensing plane of each chip paralleled. In this case, these two chips operate in differential-mode to electrically reject the effect of external angular accelerations. Assuming the bandwidth of the electrical system is much larger than the sensor's mechanical bandwidth, the overall transfer functions of the angular accelerometer and the gravity gradiometer are $T_{aa}(s) = G_{elec}H_{aa}(s)$ and $T_{gg}(s) = G_{elec}H_{gg}(s)$, respectively, where $G_{elec}$ is the gain of the electrical system. In order to characterize the developed angular-acceleration sensor, several experiments were carried out below.

First, a ring-down experiment was carried out to determine the fundamental frequency and the quality factor of the sensor by knocking the optical workbench on which the sensor was mounted. Then, the proof mass was excited by angular accelerations of the workbench. Through the amplitude decay features and fast Fourier transform (FFT) of the experimental results, the fundamental frequency of the sensor was worked out to be 27 Hz and the quality factor was 230 in air.

In order to determine the dynamic response of the prototype, a customized characterization platform was built up, as shown in Fig. 4. This platform contains two subsystems: a crank-rocker as the excitation and a pair of differential accelerometers as the reference. The basis of a crank-rocker is a classic four-bar linkage for transforming a continuous rotary motion $\omega_{AB}$ to angular oscillations $\alpha_{CD}(t) = -P \cdot \omega_{AB}^2 \cdot \sin(\omega_{AB}t)$, where the constant $P$ is determined by the geometry of the four-bar linkage mechanism.[20] A pair of off-the-shelf MEMS accelerometers were mounted on the edges of the rocking platform with a distance of $r_a$ from the central pivot. An instrumentation amplifier was used to pickup the signals from the two accelerometers. Considering the platform shakes with small angles to provide a z-axis acceleration $g(t)$ at the edge of the rocker, and the gravitational acceleration $g_0$ and the environmental acceleration along z-axis $\ddot{z}$ are exerted, the output of the differential-accelerometer system is $v_{diffacc}(t) = (v_{acc+}(t) - v_{acc-}(t)) \cdot G_{ina}$, where $v_{acc+}(t) = G_{acc} \cdot (\ddot{z} + r_a\alpha_{CD}(t) + g_0)$ and $v_{acc-}(t) = G_{acc} \cdot (\ddot{z} - r_a\alpha_{CD}(t) + g_0)$ are outputs of the accelerometers, $G_{acc}$ is the flat gain of the accelerometers within their bandwidth, $G_{ina}$ is the gain of the instrumentation amplifier. Hence, the actual angular acceleration of the crank rocker can be determined by

$$\alpha_{CD}(t) = \frac{v_{diffacc}(t)}{2r_aG_{acc}G_{ina}}. \tag{2}$$

The average gain of the accelerometers was calibrated to 120 mV/g and the mismatching was approximately 6%, the gain of the instrumentation amplifier was set to 10, and the off-center distance of 10 cm. The angular-acceleration sensor was accommodated on the characterization platform, as shown in Fig. 4(c). The sensor was driven by a sinusoidal carrier signal with a frequency of 20 kHz and an amplitude of 8 V peak-to-peak. The output of the angular-acceleration sensor consists of two parts: one is the angular element with a gain of $G_\gamma$ and the other one is the translational element with a gain of $G_L$. The translational accelerations include the environmental acceleration $\ddot{z}$, the gravitational acceleration $g_0$, and the translational acceleration $r_{gg}\alpha_{CD}(t)$ which is induced by the platform angular acceleration $\alpha_{CD}(t)$ at the location, where the angular-acceleration sensor is mounted, $r_{gg}$ away from the rotation center. Considering all the elements, the output of the sensor can be derived

$$\begin{aligned} v_{aa}(t) &= G_\gamma \cdot \alpha_{CD}(t) + G_L \cdot (\ddot{z} + r_{gg}\alpha_{CD}(t) + g_0) \\ &= \alpha_{CD}(t) \cdot (G_\gamma + G_L r_{gg}) + G_L \cdot (\ddot{z} + g_0). \end{aligned} \tag{3}$$

Benefiting from the suspension design, the compliance with respect to in-plane rotations is much larger than that of the cross-axis translational motions, so there is $G_\gamma \gg G_L$. In this case, for small off-center distances, the sensor output equation can be simplified as $v_{aa}(t) = \alpha_{CD}(t) \cdot G_\gamma$. When the rocking frequency varied from 0.6 Hz to 2.1 Hz, the outputs of this sensor were plotted with respect to the angular accelerations, as shown in Fig. 5. This prototype gave a linear response to angular accelerations with a slope of 5.8 mV/(rad/s$^2$) which is equal to the angular gain $G_\gamma$.

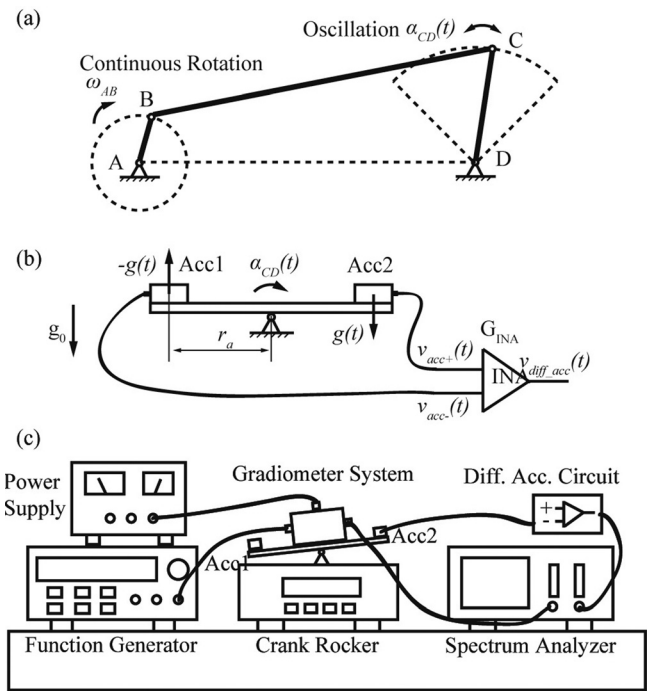


FIG. 4. Experiment setup: (a) crank rocker; (b) differential-accelerometer; (c) experiment platform.

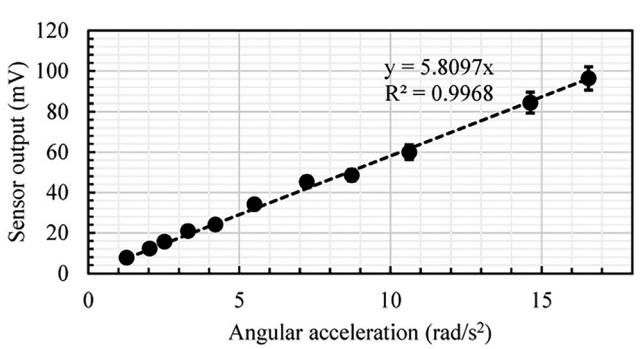


FIG. 5. The voltage outputs of the angular-acceleration sensor in terms of angular accelerations with a 6% error bar due to the mismatching of the accelerometers.

Apart from the frequency-sweep test, there is another feasible approach to determine the transfer function of the angular-acceleration sensor. During rocking at a lower frequency, the crank rocker provided auxiliary angular accelerations at higher frequencies due to the mechanical friction of hinges. Both the differential-accelerometer and the angular-acceleration sensor on the rocker coherently picked those angular-acceleration signals up. The outputs of both systems were fed into a FFT spectrum analyzer. As shown in Fig. 6(a), both the differential-accelerometer and the angular-acceleration sensor have the peaks at the rocking frequency of 0.6 Hz and higher frequencies. Recalling Equations (2) and (3), the transfer function of the angular-acceleration sensor can be worked out

$$T_{aa}(s) = 2r_a G_{acc} G_{ina} \frac{v_{aa}(s)}{v_{diffacc}(s)}. \quad (4)$$

Hence, the transfer function can be determined by the voltage ratio of the angular-acceleration sensor to the differential-accelerometer times $2r_a G_{acc} G_{ina}$. The spectrum analyzer was programmed to display the amplitude of the angular-acceleration sensor (F2) over the differential-accelerometer (F1), as shown in Fig. 6(b). The amplitudes were flat and equal to −12 dB below 10 Hz and the roll-off slope for frequencies higher than the fundamental frequency was −40 dB/decade, which agrees with the analytical model that is a classic second-order system. Based on Equation (4), the amplitude of the transfer function below 10 Hz can be derived as 6.1 mV/(rad/s$^2$), which agrees well with the angular gain $G_\gamma$ in the acceleration response experiment. In average, the sensitivity of the angular-acceleration sensor is 6 mV/(rad/s$^2$).

In addition, a preliminary noise test experiment was carried out by putting the angular-acceleration sensor on an active acceleration-free platform without any excitation. The noise equivalent angular acceleration (NEAA) can be worked out by the voltage output $v_n(s)$ over the transfer function of the angular-acceleration sensor. As shown in Fig. 7, there is a noise floor of 0.003 rad/s$^2$/$\sqrt{\text{Hz}}$ within the bandwidth of 0.1 to 10 Hz. Since the spectrum analyzer has a limited bandwidth, the large slope curve at lower frequencies was artificial. The peaks around 5 Hz were highly possibly attributed to

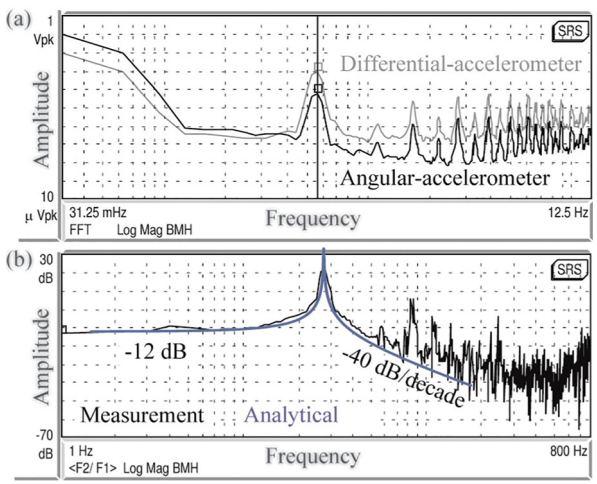


FIG. 6. Coherence sensing for determination of the transfer function.

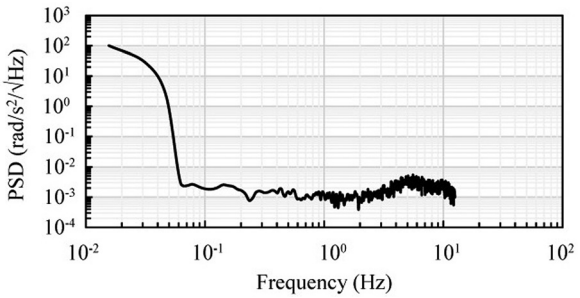


FIG. 7. Noise floor of the angular-acceleration sensor.

TABLE I. Performance comparison between this work and other angular accelerometers.

| Device | Technology | Bandwidth (Hz) | Resolution (rad/s$^2$) | Full range (rad/s$^2$) |
|---|---|---|---|---|
| This work | MEMS | 0.1–10 | 0.003 | 200 |
| Ref. 13 | MEMS | 60–200 | 0.003 | … |
| Ref. 14 | MEMS | DC-250 | 1 | 350 |
| Ref. 15 | MEMS | 30–800 | 2.5 | 200 |
| Ref. 21 | Servo | DC-100 | 0.001 | 100 |

the accelerations of the building. Compared with other sensors in Table I, this work has a comparable resolution with the conventional angular sensor but better performance than other MEMS sensors in low-frequency ranges, which is essential for those geophysical applications less than 10 Hz bandwidth.

In conclusion, this paper demonstrated a MEMS angular-acceleration sensor for low-frequency geophysical applications. This sensor can be a mechanical angular-accelerometer with the rotation angle of the proof mass sensed by the RCAT. Two orthogonally paired sensors are able to determine a component of the gravity gradient tensor by electronically reducing the effect of angular accelerations. The stator and rotor dies of the MEMS chip were fabricated simultaneously and then bonded face-to-face using flip-chip technology. The chip was wire-bonded on the front-end PCB that was then connected to the signal conditioning circuit. A ring-down experiment was carried out, showing the sensor had a fundamental frequency of 27 Hz and a quality factor of 230 in air. A customized characterization platform was built up to investigate the response to angular accelerations and the transfer function of the sensor, both giving a sensitivity of 6 mV/(rad/s$^2$). A noise test experiment demonstrated a noise floor of 0.003 rad/s$^2$/$\sqrt{\text{Hz}}$ within a bandwidth of 0.1 Hz to 10 Hz, which is comparable with the conventional sensor and better than other MEMS angular-acceleration sensors. The miniaturized angular-acceleration sensor has a low cost, a high sensitivity and a low noise floor at low frequencies, which opens up the possibility of large-scale and economic deployments for geophysical explorations on unmanned vehicles or as a payload for space missions.

[1]L. A. Lines, C. L. Mauldin, J. W. Hill, and R. A. Aiello, in *SPE Annual Technical Conference and Exhibition* (Society of Petroleum Engineers, 2014).
[2]A. Mat-Isa and M. Usher, Geophys. J. Int. **109**, 197 (1992).
[3]M. V. Moody, H. J. Paik, and E. R. Canavan, Rev. Sci. Instrum. **74**, 1310 (2003).

[4]W. J. Hinze, R. R. Von Frese, and A. H. Saad, *Gravity and Magnetic Exploration: Principles, Practices, and Applications* (Cambridge University Press, 2013).
[5]D. DiFrancesco, A. Grierson, D. Kaputa, and T. Meyer, Geophys. Prospect. **57**, 615 (2009).
[6]R. H. Dixon and J. Bouchaud, in *MOEMS-MEMS 2006 Micro and Nanofabrication* (International Society for Optics and Photonics, 2006), p. 611306.
[7]H. Huang, B. Carande, R. Tang, J. Oiler, D. Zaitsev, V. Agafonov, and H. Yu, Appl. Phys. Lett. **102**, 193512 (2013).
[8]D. Yamane, T. Konishi, T. Matsushima, K. Machida, H. Toshiyoshi, and K. Masu, Appl. Phys. Lett. **104**, 074102 (2014).
[9]T. Deng, D. Chen, J. Wang, J. Chen, and W. He, J. Microelectromech. Syst. **23**, 92 (2014).
[10]J. Laine and D. Mougenot, in *Transducers 2007* (2007), pp. 1473–1477.
[11]W. T. Pike, A. K. Delahunty, A. Mukherjee, G. Dou, H. Liu, S. Calcutt, and I. Standley, in *IEEE Sensors 2014 Proceedings* (2014), pp. 1599–1602.
[12]W. T. Pike, S. Calcutt, I. Standley, A. Mukherjee, J. Temple, T. Warren, C. Charalambous, H. Liu, A. Stott, and J. McClean, in *Lunar and Planetary Science Conference* (2016), Vol. 47, p. 2081.
[13]M. Projetti, O. Vancauwenberghe, H. Paulson, N. Goujon, F. Marty, and D. Aubry, in *IEEE Sensors 2014* (IEEE, 2014), pp. 1595–1598.
[14]G. J. O'Brien, D. J. Monk, and K. Najafi, in *Transducers 2003* (2003), Vol. 2, pp. 1371–1374.
[15]A. Gola, N. Bagnalasta, P. Bendiscioli, E. Chiesa, S. Delbò, E. Lasalandra, F. Pasolini, M. Tronconi, T. Ungaretti, and A. Baschirotto, in *Proceedings of the 27th European Solid-State Circuits Conference, ESSCIRC 2001* (2001), pp. 321–324.
[16]R. Feynman, R. Leighton, and M. Sands, *The Feynman Lectures on Physics: The New Millennium Edition: Mainly Mechanics, Radiation, and Heat* (Basic Books, 2011), Vol. 1.
[17]H. Liu, W. T. Pike, and G. Dou, J. Appl. Phys. **119**, 124508 (2016).
[18]V. Kaajakari, *Practical MEMS: Design of Microsystems, Accelerometers, Gyroscopes, RF MEMS, Optical MEMS, and Microfluidic Systems* (Small Gear Publishing, 2009).
[19]S. Beeby, G. Ensell, M. Kraft, and N. White, *MEMS Mechanical Sensors* (Artech House, 2004).
[20]F. Y. Chen, J. Eng. Ind. **91**, 45 (1969).
[21]Jewell, ASXC Series Angular Accelerometers, datasheet.